Analytical representation of flows due to arbitrary singularity distributions for wave diffraction radiation by offshore structures in water of finite depth

Huiyu Wu, Jiayi He, Francis Noblesse

School of Naval Architecture, Ocean & Civil Engineering, Shanghai Jiao Tong University, Shanghai, China.
Email: why2277@sjtu.edu.cn

1. Introduction

Diffraction radiation of regular waves by offshore structures is usually considered within the framework of the classical Green-function and boundary-integral method, also called panel method, related to potential-flow theory for deep water and the more general and considerably more difficult case of uniform finite water depth analyzed in this study.

Within this classical theoretical framework, the flow around an offshore structure is represented by means of distributions of singularities (sources and dipoles) over the surface of the offshore structure. Accurate and efficient numerical evaluation of flows created by (typically polynomial, notably constant, linear or quadratic) distributions of singularities over (flat or curved) panels of arbitrary shape (notably triangular and quadrilateral) approximating the surface of an offshore structure is then a major element of every panel method. This core element of the Green-function and boundary-integral method is crucial as it largely determines the accuracy and the efficiency of a panel method, and is considered in this study for diffraction radiation of regular waves in finite water depth, including the special case of deep water.

1.1 The classical direct Green-function method

The 'direct Green-function method', in which the Green function and its derivatives are first evaluated and subsequently integrated over the panels that approximate the surface of the structure, is commonly adopted for wave diffraction radiation by offshore structures. Accordingly, the corresponding Green function has been extensively studied, as is reviewed in [1-4], especially in the simpler case of deep water.

However, the Green function for diffraction radiation of regular waves is considerably more complicated in water of finite depth than in deep water. In particular, G and ∇G are functions of two variables (nondimensional coordinates) in deep water, but are functions of four variables (the water depth d, the horizontal distance $h = \sqrt{(x-\xi)^2 + (y-\eta)^2}$ between the point source $\boldsymbol{\xi}$ and the flow-field point $\mathbf{x}$ and the vertical coordinates z and ζ) in finite water depth.

Moreover, the Green function G is usually decomposed into a wave component G^W and a local-flow component G^L that represent the circular waves created by the pulsating source or a non-oscillatory local flow. Although the sum $G^W + G^L$ is a smooth function, the components G^W and G^L are not smooth above the source point.

Lastly, the local-flow components G^L and ∇G^L have complicated singularities at the mirror image of the point source about the undisturbed free surface. E.g., the deep-water local-flow component G^L includes a logarithmic singularity [1,2] and numerical integrations of the singular functions G^L and ∇G^L over a panel require a complicated special treatment; e.g. [5].

Thus, the 'direct Green-function method', although widely used and well established in offshore hydrodynamics, involves significant mathematical and numerical complexities, especially for the case of finite water-depth considered in this study.

1.2 The Fourier-Kochin method

An analytical representation of the flow created by a general distribution of singularities over a hull-surface panel is given in this study for wave diffraction radiation by offshore structures in finite water depth. This flow-representation is based on the Fourier-Kochin (FK) approach, in which space-integration over the panel is performed first and Fourier-integration is performed subsequently, unlike the common 'direct Green-function method' in which the Green function (defined via a Fourier integration) is evaluated first and subsequently integrated over the panel. The mathematical and numerical complexities associated with the evaluation of the Green function G and its derivatives are then avoided within the FK approach, in which numerical evaluation of G and ∇G is bypassed and the flow potential due to a distribution of sources and dipoles (singularities) is evaluated directly, as is also explained in [6-9] and other studies.

A compelling advantage of this approach is that the space-integration over a panel merely amounts to integrating an elementary (exponential-trigonometric) function, a trivial task that can be performed very accurately and efficiently (analytically for polynomial distributions of sources and dipoles over flat panels).

However, as is shown in Section 3, the Fourier-Kochin approach requires evaluation of a singular double Fourier integral that accounts for free-surface effects, evidently a nontrivial task. This task is analyzed in [6] for an arbitrary distribution of singularities and arbitrary dispersion functions related to particular classes of dispersive waves. Applications of the general analysis given in [6] to steady ship waves and wave diffraction radiation by offshore structures in deep water given in [6], to ship motions in deep water given in [7,8] and to diffraction radiation of regular waves by offshore structures in finite water depth given in this study yield analytical representations of flows created by general distributions of singularities for specific dispersion relations and corresponding particular classes of flows in ship and offshore hydrodynamics.

The resulting analytical flow-representation for wave diffraction radiation by offshore structures in finite water depth given in the study provides a mathematically-exact smooth decomposition of free-surface effects into a nonoscillatory local flow and waves. The waves in this flow decomposition are defined by a regular single Fourier integral, and the local flow is given by a double Fourier integral with a smooth integrand that only involves ordinary functions and is dominant within a compact region near the origin of the Fourier plane. Illustrative numerical applications for typical distributions of sources and dipoles over a panel show that the flow-representation given in the study is well suited for practical numerical evaluations.

2. Rankine-Fourier decomposition of the Green function

The Green function associated with diffraction radiation of regular waves of frequency ω in water of uniform finite depth D and large horizontal extent is now considered. The gravitational acceleration is denoted as g. A Cartesian system of coordinates (X, Y, Z) is used. The Z axis is vertical and points upward, and the undisturbed free surface is taken as the plane $Z = 0$. The nondimensional coordinates $\mathbf{x}$, water depth d and frequency f are defined as

$$\mathbf{x} \equiv (x, y, z) \equiv (X, Y, Z)/L \ , \ \ d \equiv D/L \ \text{ and } \ f \equiv \omega\sqrt{L/g} \ . \tag{1}$$

The reference length L may be taken as a characteristic length L_s of a structure, or as the water depth D or the length g/ω^2 related to the wavelength of the waves created by the body. The choice of reference length $L = g/\omega^2$ yields $f \equiv 1$.

The Green function $G(\mathbf{x}, \boldsymbol{\xi}; f, d)$ represents the potential of the flow created at a point $\mathbf{x} \equiv (x, y, -d \le z \le 0) \equiv (h\cos\psi, h\sin\psi, z)$ by a pulsating source located at a point $\boldsymbol{\xi} \equiv (\xi, \eta, -d < \zeta < 0)$, and can be expressed as

$$4\pi G = G^S + G^F \tag{2}$$

where G^S is expressed in terms of elementary free-space singularities (Rankine sources) and the component G^F is given by a singular double Fourier integral. Alternative Rankine components G^S in the Rankine-Fourier decomposition (2) have been used in the literature. The Rankine component G^S in (2) is chosen here as

$$G^S = -1/r - 1/r_d - 1/r' - 1/r'_d + 2/r^f + 2/r^f_d \ \text{ where } \ r \equiv\sqrt{\rho^2 + (z-\zeta)^2} \ , \ \ r_d \equiv\sqrt{\rho^2 + (z+\zeta+2d)^2} \ , \tag{3a}$$

$$r' \equiv\sqrt{\rho^2 + (z+\zeta)^2} \ , \ \ r'_d \equiv\sqrt{\rho^2 + (z-\zeta-2d)^2} \ , \ \ r^f \equiv\sqrt{\rho^2 + (z+\zeta-1/f^2)^2} \ , \ \ r^f_d \equiv\sqrt{\rho^2 + (z-\zeta-1/f^2-2d)^2} \tag{3b}$$

with $\rho \equiv\sqrt{(x-\xi)^2 + (y-\eta)^2}$. The Fourier component G^F in (2) is given by

$$G^F = \frac{f^2}{\pi}\int_{-\pi}^{\pi} d\gamma \int_0^\infty dk \, \frac{A^G \, \mathcal{E} \, e^{\,\mathrm{i}\,k\,h\cos(\gamma-\psi)}}{f^2 - k\tanh(kd) + \mathrm{i}\,\epsilon f} \ \text{ where } \ \mathcal{E} \equiv e^{-\,\mathrm{i}\,k\,(\xi\cos\gamma + \eta\sin\gamma)}\cosh[k(\zeta+d)]/(e^{kd}/2) \ , \tag{4a}$$

$$A^G \equiv (k/f^2+1)\cosh[k(z+d)]/[2\cosh(kd)] + [1 - k\tanh(kd)/f^2](1/2 - e^{-k/f^2})\, e^{kz} \tag{4b}$$

and $\epsilon = +0$. In the Fourier plane (k, γ) where $-\pi \le \gamma \le \pi$, the dispersion relation $f^2 - k\tanh(kd) = 0$ defines a single dispersion circle $k = k^*$ where k^* is the positive real root of the dispersion equation

$$k^*\tanh(k^*d) = f^2 \ . \tag{5}$$

Expression (4b) for the amplitude function A^G that corresponds to the Rankine component G^S defined by (3) shows that one has $A^G \to 0$ as $k \to 0$ and $A^G \to 1$ as $k \to \infty$ for $z = 0$, whereas the amplitude function that corresponds to the Rankine component $G^S = -1/r - 1/r_d$ widely used in the literature does not vanish at $k = 0$ and is unbounded as $k \to \infty$ if $z = 0$. The Rankine component G^S given by (3) is then clearly preferable to the classical Rankine component given in the literature.

Indeed, the Rankine-Fourier decomposition (2) where the Rankine component G^S is taken as (3) and the Fourier component G^F is given by (4) is a major element of the flow-representation given in the study, and differs from the similar decompositions given in the literature.

3. Fourier-Kochin representation of the free-surface flow created by a general distribution of singularities

The Green-function and boundary-integral method requires evaluation of the flow potentials

$$\phi_p(\mathbf{x}) = \int_{\mathcal{H}_p} \left\{ \begin{matrix} \sigma(\boldsymbol{\xi})\, G(\mathbf{x}, \boldsymbol{\xi}) \\ \delta(\boldsymbol{\xi})\, \mathbf{n}(\boldsymbol{\xi}) \cdot \nabla_{\boldsymbol{\xi}} G(\mathbf{x}, \boldsymbol{\xi}) \end{matrix} \right\} da(\boldsymbol{\xi}) \ , \ \text{where } \ \nabla_{\boldsymbol{\xi}} \equiv (\partial/\partial\xi, \partial/\partial\eta, \partial/\partial\zeta) \ , \tag{6}$$

associated with distributions of sources and dipoles, with densities denoted as σ or δ in (6), over (flat or curved) panels $\mathcal{H}_p$ of various shapes (notably triangle or quadrilateral) that are used to approximate the surface of a body (offshore structure or ship). Accurate evaluation of the flow potential ϕ_p defined by (6) is a basic and crucial core issue of the panel method.

The Rankine-Fourier decomposition (2) of G shows that the flow potential $\phi_p(\mathbf{x})$ defined by (6) can be expressed as

$$\phi_p(\mathbf{x}) = \phi^S_p(\mathbf{x}) + \phi^F_p(\mathbf{x}) \tag{7}$$

where $\phi^S_p(\mathbf{x})$ and $\phi^F_p(\mathbf{x})$ correspond to the Rankine and Fourier components G^S or G^F in (2).

The Rankine potential ϕ^S_p in (7) can be evaluated via cubature formulae without difficulties, and is then ignored hereafter. However, evaluation of the contribution of the Fourier component G^F in (2) is a nontrivial task because the Fourier component G^F defined by (4) and its gradient $\nabla_{\boldsymbol{\xi}} G^F$ are relatively difficult to evaluate accurately and efficiently, especially for finite water depth, and moreover involve complicated singularities that are difficult to integrate accurately over a panel [5].

An alternative method for evaluating the Fourier component ϕ^F_p that corresponds to the flow potential ϕ_p defined by (6) is then considered hereafter. This method is based on the Fourier-Kochin method, as is now explained.

Expressions (4) for the Fourier component G^F in the representation (2) of G show that the flow potential $\phi^F_p(\mathbf{x})$ associated with a given distribution of singularities (sources or dipoles) over a panel $\mathcal{H}_p$ centered at $\boldsymbol{\xi}_p \equiv (\xi_p, \eta_p, \zeta_p)$ is given by

$$4\pi\,\phi^F_p(\mathbf{x}) = \frac{f^2}{\pi}\int_{-\pi}^{\pi} d\gamma \int_0^\infty dk \, \frac{A^G A_p \, e^{\,\mathrm{i}\,k\,h_p\cos(\gamma-\psi_p)}}{f^2 - k\tanh(kd) + \mathrm{i}\,\epsilon f} \tag{8}$$

where $h_p \equiv\sqrt{(x-\xi_p)^2 + (y-\eta_p)^2}$, $(\cos\psi_p, \sin\psi_p) \equiv (x-\xi_p, y-\eta_p)/h_p$ and A^G is defined by (4b). Moreover, A_p is given by

$$A_p = \int_{\mathcal{H}_p} \left\{ \begin{matrix} \sigma(\boldsymbol{\xi}) \\ k\, a_p\, \delta(\boldsymbol{\xi}) \end{matrix} \right\} \mathcal{E}_p \, da(\boldsymbol{\xi}) \ \text{ where } \ a_p \equiv n^z \tanh[k(\zeta+d)] - \mathrm{i}\,(n^x\cos\gamma + n^y\sin\gamma) \tag{9a}$$

$$\text{and}\ \ \mathcal{E}_p \equiv e^{-\mathrm{i}\,k\,[(\xi-\xi_p)\cos\gamma+(\eta-\eta_p)\sin\gamma)]}\cosh[k(\zeta+d)]/(e^{kd}/2)\ . \tag{9b}$$

The amplitude (Kochin) functions A_p defined by (9) are determined via integrations of the elementary wave function $\mathcal{E}_p$ over the panel $\mathcal{H}_p$. Expression (9b) shows that $\mathcal{E}_p$ does not oscillate rapidly for a panel of reasonable size. The function A_p can then be evaluated accurately and efficiently for general distributions of sources or dipoles with densities σ or δ.

Indeed, the surface integration of the slowly-varying smooth elementary functions $\sigma\,\mathcal{E}_p$ or $k\,a_p\,\delta\,\mathcal{E}_p$ over a panel $\mathcal{H}_p$ required in (9a) is incomparably simpler than the integration of the highly singular functions G^F and $\nabla_{\boldsymbol{\xi}} G^F$ required in (6) associated with the direct Green-function method, and this basic difference is a compelling advantage of the Fourier-Kochin approach.

4. Practical analytical representation of the flow created by a general distribution of singularities

For simplicity, the subscript p in (8) is ignored in this section, where the flow potential ϕ^F defined by (8) is considered for an arbitrary amplitude (Kochin) function A. The integrand of the double Fourier integral (8) is singular at the dispersion curve $f^2-k\tanh(kd)=0$, and accurate and efficient evaluation of this singular double Fourier integral is then nontrivial.

This crucial issue is considered in [9]. Specifically, the singular double Fourier integral (8) is decomposed as

$$4\pi\,\phi^F(\mathbf{x}) = \phi^W(\mathbf{x}) + \phi^L(\mathbf{x}) \tag{10}$$

where ϕ^W represents the waves that are contained in the flow potential ϕ^F, and ϕ^L is a non-oscillatory local flow that vanishes rapidly in the far field. Moreover, the integrand of the double Fourier integral ϕ^L is smooth everywhere (notably at the dispersion circle), decays rapidly as the wavenumber $k\to\infty$ and is dominant at or near the origin $k=0$ of the Fourier plane.

4.1 Wave potential ϕ^W

The wave component ϕ^W in the flow decomposition (10) of the flow potential ϕ^F is given by a single Fourier integral along the dispersion circle $k=k^*$. One has

$$\frac{\phi^W}{f^2} \equiv -\mathrm{i}\,P\int_{\psi-\pi/2}^{\psi+\pi/2}[(1+\Theta)\,A^*\,e^{\,\mathrm{i}\,\varphi}+(1-\Theta)\,\overline{A^*}\,e^{-\mathrm{i}\,\varphi}]\,d\gamma\ \ \text{where}\ \ P\equiv\frac{e^{k^*d}\cosh[k^*(z+d)]}{2\sinh^2(k^*d)+2f^2d}\ , \tag{11a}$$

$$\Theta\equiv\mathrm{erf}\,(\varphi/\mu_*)\ \ ,\ \ \varphi\equiv k^*h\cos(\gamma-\psi)\ \ ,\ \ A^*\equiv A(k=k^*,\gamma) \tag{11b}$$

and an overline means complex conjugate. One has $0\le\Theta\le 1$ within the integration range $\psi-\pi/2\le\gamma\le\psi+\pi/2$.

In the deep-water limit $d\to\infty$, one has $k^*=f^2$ and $P=e^{f^2z}$, and expressions (11) agree with the expressions for the wave potential ϕ^W given in [6].

4.2 Wave component in the Green function

In the limit $\mu_*=+0$ and in the special case $A(k=k^*,\gamma)=\cosh[k^*(\zeta+d)]/(e^{k^*d}/2)$ that corresponds to a point source located at $\boldsymbol{\xi}\equiv(0,0,\zeta)$, the wave component ϕ^W in (11) becomes

$$\phi^W/f^2 = 2\,\pi\,A^W\,[\widetilde{H}_0(k^*h)-\mathrm{i}\,J_0(k^*h)]\ \ \text{where}\ \ A^W\equiv\cosh[k^*(z+d)]\cosh[k^*(\zeta+d)]\,/\,[\sinh^2(k^*d)+f^2d] \tag{12}$$

This expression agrees with the expression for the wave component in the Green function associated with diffraction radiation of regular waves in finite water depth.

In deep water, one has $A^W=1$, and expression (12) agrees with the wave component of the Green function given in [1,2].

4.3 Local-flow potential ϕ^L

The local-flow potential ϕ^L that corresponds to the potential ϕ^F determined by the singular double Fourier integral (8) is given by a regular double Fourier integral

$$\frac{\phi^L}{f^2}\equiv\frac{2}{\pi}\,\mathrm{Re}\int_{\psi-\pi/2}^{\psi+\pi/2}d\gamma\int_0^\infty dw\,A^R(w,\gamma)\,e^{\,\mathrm{i}\,wk^*h\cos(\gamma-\psi)}\ \ \text{where} \tag{13a}$$

$$A^R=\frac{A^GA}{f^2/k^*-w\tanh(wk^*d)}-P\left[\frac{e^{-\mu_*^2\,(1-w)^2/4}}{1-w}\,A^*+\frac{e^{-\mu_*^2\,(1+w)^2/4}}{1+w}\,\overline{A^*}\right]\ \ \text{with} \tag{13b}$$

$$A^G\equiv(wk^*/f^2+1)\cosh[wk^*(z+d)]\,/\,[2\cosh(wk^*d)]+(1/2-e^{-wk^*/f^2})\,[1-(wk^*/f^2)\tanh(wk^*d)]\,e^{wk^*z}\ . \tag{13c}$$

Moreover, one has $A\equiv A(w,\gamma)$ and $A^*\equiv A(w=1,\gamma)$ in (13b), P in (13b) is given by (11a), and $w\equiv k/k^*$ in (13). The function $A_*^R\equiv A^R(w=1,\gamma)$ is finite at the dispersion circle $w=1$ and given by

$$A_*^R=-P\,(\,\widehat{\Gamma}\,A^*+e^{-\mu_*^2}\,\overline{A^*}/2+A_w^*)+(k^*/f^2)\,(1/2-e^{-k^*/f^2})\,A^*\,e^{k^*z} \tag{13d}$$

where $\widehat{\Gamma}\equiv k^*(z+d)\tanh[k^*(z+d)]+1/(1+f^2/k^*)-f^2d\cosh^2(k^*d)\,/\,[\sinh^2(k^*d)+f^2d]$ and $A_w^*\equiv A_w(w=1,\gamma)$.

In the deep-water limit $d\to\infty$, one has $w\equiv k/f^2$ and

$$A^R=\frac{A^GA}{1-w}-e^{f^2z}\left[\frac{e^{-\mu_*^2\,(1-w)^2/4}}{1-w}\,A^*+\frac{e^{-\mu_*^2\,(1+w)^2/4}}{1+w}\,\overline{A^*}\right]\ \ \text{where}\ \ A^G\equiv[1+(w-1)\,e^{-w}]\,e^{wf^2z}\ .$$

At the dispersion circle $w=1$, the function $A_*^R\equiv A^R(w=1,\gamma)$ is given by $A_*^R=-[(e^{-1}+f^2z)\,A^*+e^{-\mu_*^2}\,\overline{A^*}/2+A_w^*]\,e^{f^2z}$. The foregoing expressions for deep water agree with the expressions given in [6].

Expressions (11b) and (13b) involve a parameter μ_*. Thus, both the wave component ϕ^W and the local-flow component ϕ^L in the waves and local-flow decomposition (11) and (13) depend on μ_*, and the flow-representation (11) and (13) therefore defines a family of alternative decompositions into waves and local flows; i.e., different choices of μ_* yield alternative

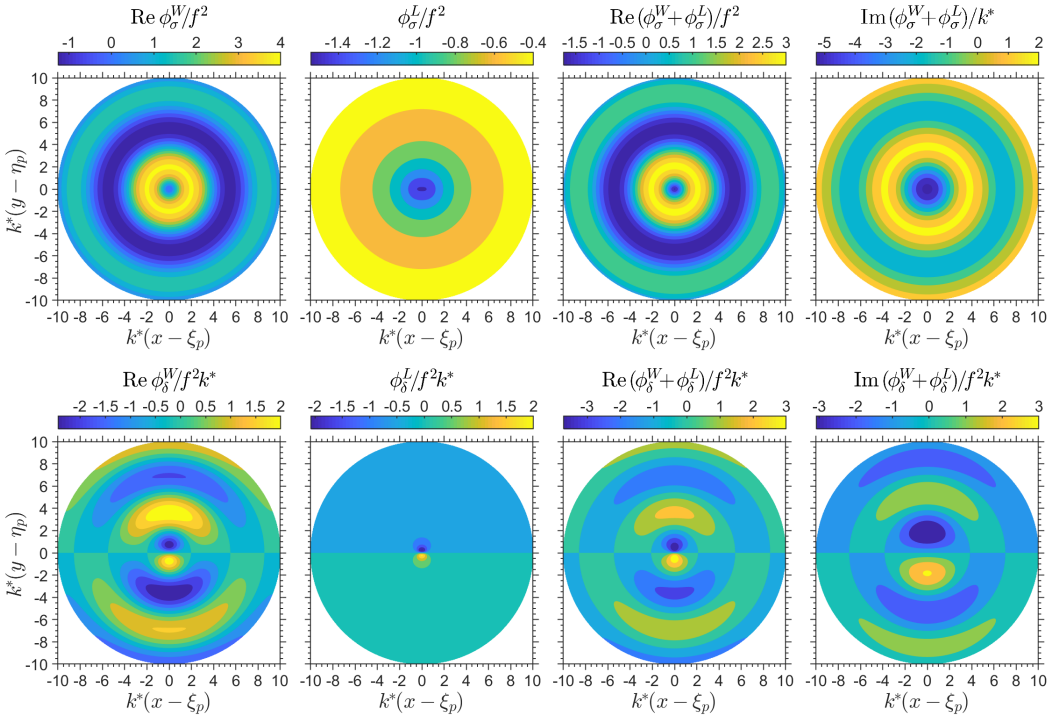

Figure 1: The top row depicts contour plots of the flow potentials Re ϕ_σ^W (left column), ϕ_σ^L, Re $(\phi_\sigma^W+\phi_\sigma^L)$, Im ϕ_σ^W (right) associated with a source distribution for $\mu_*=0.5$ and $f^2d=1$ within the region $k^*h_p \equiv k^*[(x-\xi_p)^2+(y-\eta_p)^2]^{1/2} \leq 10$ with $k^*z=-\pi/30$. The bottom row similarly depicts the potentials Re ϕ_δ^W (left), ϕ_δ^L, Re $(\phi_\delta^W+\phi_\delta^L)$, Im ϕ_δ^W (right) for a dipole distribution.

decompositions of the flow potential ϕ^F into a wave potential ϕ^W and a local-flow potential ϕ^L. Indeed, flow decompositions into wave and local-flow components are not unique.

The flow-representation given by (10), (11) and (13) does not involve approximations, i.e. is mathematically exact, and the flow potential ϕ^F given by (8) is then independent of the parameter μ_* that appears in both the wave potential ϕ^W and the local-flow potential ϕ^L. The parameter μ_* can then be chosen arbitrarily from a strictly mathematical standpoint.

However, from the practical standpoint of numerical evaluation, the parameter μ_* must not be chosen too large (because the local-flow potential ϕ^L contains waves within a large region if μ_* is large) or too small (to avoid excessively sharp variations of the wave and local-flow potentials ϕ^W and ϕ^L at the origin). The numerical study for typical distributions of sources and dipoles over a panel to be presented at the Workshop shows that the choice $\mu_* \approx 0.5$ yields a smooth flow decomposition in which the local-flow potential ϕ^L is non-oscillatory and mostly significant within a relatively small near-field region. This choice is consistent with the mathematical and numerical studies reported in [6-9], and may be considered as nearly optimal.

5. Numerical illustration and verification

For purposes of illustration and verification, uniform distributions of sources and dipoles over a rectangular panel $\mathcal{H}_p$ located in the vertical plane $\eta=\eta_p$ and defined as $-\delta_\xi \leq \xi-\xi_p \leq \delta_\xi$ and $-\delta_\zeta \leq \zeta \leq 0$ are considered. The top side of the panel $\mathcal{H}_p$ touches the free surface $\zeta=0$. One has $(n^x,n^y,n^z)=(0,1,0)$ on $\mathcal{H}_p$. The densities σ and δ of the distributions of sources and dipoles are taken equal to $1/(2\,\delta_\xi\,\delta_\zeta)$, which corresponds to a unit source or dipole uniformly distributed over the area of $\mathcal{H}_p$. The length and the height of $\mathcal{H}_p$ are chosen as $\delta_\xi=C^x/k^*$ and $\delta_\zeta=C^z/k^*$ with $C^x=\pi/10$ and $C^z=\pi/15$.

The flow potentials associated with the source and dipole distributions are depicted in Fig.1. Additional numerical illustrations and verifications will be reported at the Workshop.

References

[1] F. Noblesse, The Green function in the theory of radiation and diffraction of regular water waves by a body, J. Eng. Math. 16 (2) (1982) 137-169.

[2] H. Wu, C. Zhang, Y. Zhu, W. Li, D. Wan, F. Noblesse, A global approximation to the Green function for diffraction radiation of water waves, Eur. J. Mech. B Fluids 65 (2017) 54-64.

[3] C. Xie, Y. Choi, F. Rongère, A. Clément, G. Delhommeau, A. Babarit, Comparison of existing methods for the calculation of the infinite water depth free-surface Green function for the wave-structure interaction problem, Appl. Ocean Res. 91 (2018) 150-163.

[4] E. Mackay, Consistent expressions for the free-surface Green function in finite water depth, Appl. Ocean Res. 93 (2019) 101965.

[5] Y. Liu, J.M. Falzarano, A method to remove irregular frequencies and log singularity evaluation in wave-body interaction problems, J. Ocean Eng. Mar. Energy 3 (2017) 161-189.

[6] J. He, H. Wu, R.-C. Zhu, C.-J. Yang, F. Noblesse, Practical flow-representations for arbitrary singularity-distributions in ship and offshore hydrodynamics, with applications to steady ship waves and wave diffraction-radiation by offshore structures, Eur. J. Mech. B Fluids 83 (2020) 24-41.

[7] J. He, H. Wu, R.-C. Zhu, C.-J. Yang, F. Noblesse, Practical evaluation of flows due to arbitrary singularity distributions in the 3D theory of ship motions in regular waves at $\tau < 1/4$, Eur. J. Mech. B Fluids 83 (2020) 212-225.

[8] J. He, H. Wu, R.-C. Zhu, C.-J. Yang, F. Noblesse, Practical evaluation of flows due to arbitrary singularity distributions in the 3D theory of ship motions in regular waves at $0.3 \leq \tau$, Eur. J. Mech. B Fluids 85 (2021) 8-20.

[9] H. Wu, J. He, R.-C. Zhu, C.-J. Yang, F. Noblesse, Practical representation of flows due to general singularity distributions for wave diffraction-radiation by offshore structures in finite water depth, submitted to Eur. J. Mech. B Fluids.